Cuttlefish Turn Slowly but Tightly with Directional Flexibility Using Short Vortex Ring Jets

Alissa M. Ganley[1,*], Paul S. Krueger[2], and Ian K. Bartol[1]

[1] Department of Biological Sciences, Old Dominion University, Norfolk, Virginia
[2] Department of Mechanical Engineering, University of North Texas, Denton, Texas

Abstract

Cephalopods, such as squids and cuttlefishes, play an integral role in food web dynamics as both prey and predator, whereby proficient turning is required for successful predator avoidance and prey capture. However, surprisingly little is known about the turning capabilities of most cephalopods. In this study, body movements and 3D flow fields around adult dwarf cuttlefish, Sepia bandensis*, were recorded during a range of maneuvers to quantify turning performance. While significant variation in turning capabilities was observed,* S. bandensis*, on average, turned tightly (mean length-specific turning radius = 0.14 ± 0.013 [SEM]; minimum length-specific turning radius = 0.013 ± 0.002) but relatively slowly (average angular velocity = 45.85° ± 2.70° s^{-1}; maximum angular velocity = 110.34° ± 7.09° s^{-1}). Jet properties were not reliable predictors of turn performance, as* S. bandensis *relied primarily on short vortex ring jets (length-to-diameter ratio of jet vorticity = 2.47 ± 0.18) of moderate velocity (average jet velocity 14 cm s^{-1}; maximum jet velocity 22 cm s^{-1}) irrespective of turn type. The orientation of the turn (arms-first vs. tail-first) did not have a significant effect on kinematic or hydrodynamic properties, and most turns were performed arms-first (72.6% of turns). Compared to other cephalopods, cuttlefish turned using shorter jets with similar velocity profiles. These results are consistent with the residence of* S. bandensis *in complex benthic habitats, where tight, controlled turns facilitated by short jet pulses and high turning proficiency in either orientation are needed.*

Introduction

Turning is an important part of life in the oceans, necessary for capturing prey, avoiding predators, navigating complex habitats, and communicating with conspecifics (Hanlon and Messenger, 1996; Hanlon *et al.*, 2018; Bartol *et al.*, 2022). Turning performance has been examined in a range of taxa, including fishes, beetles, squids, and turtles (Weihs, 1972; Webb and Kostecki, 1984; Fuiman and Webb, 1988; Blake *et al.*, 1995; Budick and O'Malley, 2000; Walker, 2000; Drucker and Lauder, 2001; Fish and Nicastro, 2003; Fish *et al.*, 2003; Müller and Lentink, 2004; Rivera *et al.*, 2006; Danos and Lauder, 2007; Porter *et al.*, 2011; Jastrebsky *et al.*, 2016, 2017; Bartol *et al.*, 2022, 2023; Ganley *et al.*, 2023). Studies integrating kinematic data with flow quantification data have provided valuable insights for understanding turning, as they link body movements to momentum transfer to the surrounding medium. For example, Epps and Techet (2007) found that giant danios (*Danio aequipinnatus*) use both maneuvering (initial) and propulsive (secondary) vortices to achieve C-start turns. Sunfish (*Lepomis macrochirus*) modify impulse and the timing of shed vortex rings to produce turns of differing strength,

Received 8 November 2024; Accepted 1 February 2026; Published online 8 April 2026.
* Corresponding author. Present address: Ecosystem Health Section, Virginia Institute of Marine Science, William & Mary, Gloucester Point, Virginia; email: alissaganley@gmail.com.
Abbreviations: COR, center of rotation; DDPTV, defocusing digital particle tracking velocimetry.

Correction: Several of the authors' proof corrections, including a few changes to the temperature data, were not incorporated into the ahead of print publication of the article posted on April 8, 2026. The final online and print editions contain all changes.

The Biological Bulletin, February 2025, volume 248, number 1: 47–62. https://doi.org/10.1086/740963

speed, and tightness (Drucker and Lauder, 2001). Müller *et al.* (2008) analyzed the flow around larval zebrafish (*Danio rerio*) during routine turns and found that two sets of vortex rings are shed in rows on either side of the body, similar to patterns observed in anguilliform swimmers. During these turns, the wake is large and vortex ring circulation is short-lived, as expected for flows at intermediate Reynolds numbers. Thandiackal and Lauder (2020) found that turns in *D. rerio* are powered mainly by positive work done on the water by the posterior body region. However, 10%–20% of the total work performed during turning is negative work (from the fluid onto the body), which occurs anteriorly. This pattern is different from steady swimming, where positive work is generated at the tail end of the animal (Rome *et al.*, 1993; Johnson *et al.*, 1994; Jayne and Lauder, 1995; Coughlin and Rome, 1996; Coughlin, 2000; Ellerby *et al.*, 2022).

In addition to studies of fishes, dual (kinematics + hydrodynamics) analyses have been used to understand turning in jet-propelled animals. In the moon jelly, *Aurelia aurita*, hydrodynamic and kinematic analyses revealed that nonuniform bell contractions produce asymmetric vortex rings to effect turns (Gemmell *et al.*, 2015), which differ from the symmetric vortex structures produced during rectilinear swimming (Dabiri *et al.*, 2005; Dabiri, 2009; Colin *et al.*, 2013). The vortex rings produced on the inside of the turn are often interconnected, similar to flows produced by some fish (Lauder and Drucker, 2002; Linden and Turner, 2004) and squids (Bartol *et al.*, 2018, 2022, 2023). Conversely, siphonophores employ the same jet patterns used during rectilinear swimming, only nectophores toward the apex of the colony are positioned at an angle with respect to the rest of the nectosome, providing flows with sufficient torque for turning (Costello *et al.*, 2015).

Jet-propelled cephalopods, such as squids, have flexible funnels that vector jet flows in different directions below the animal, allowing for swimming in either arms-first (forward) or tail-first (backward) orientations. When turning, orientation plays a significant role, with many squids completing tight but slow arms-first turns and fast but broad tail-first turns, although some species diverge from this general pattern (Bartol *et al.*, 2022, 2023; Ganley *et al.*, 2023). Squid use two main "jet modes" while swimming: jet mode I, where a short plug of water is ejected from the funnel, creating one discrete vortex ring, and jet mode II, where a longer, more sustained jet is produced with a leading vortex ring structure and a trailing jet (Bartol *et al.*, 2009a). There is a predictable transition between the two jet modes that occurs when the length-to-diameter ratio of the jet vorticity field (L_ω/D_ω) is ~3–4 (Bartol *et al.*, 2009a, 2022, 2023). In mechanical jet systems, this transition is known as the formation number (F) (Gharib *et al.*, 1998; Krueger and Gharib, 2003). This formation number occurs at the point of maximal circulation before the vortex ring "pinches off" and no longer entrains flow from the original jet (Gharib *et al.*, 1998; Krueger and Gharib, 2003). During turns, squids often use multiple jet mode I pulses, as shorter, more controlled jets are beneficial for tight turning. This mode is frequently favored when moving arms-first (Bartol *et al.*, 2022, 2023; Ganley *et al.*, 2023). Jet mode II pulses are often higher in jet velocity and impulse and drive high-angular-velocity broad turns (Bartol *et al.*, 2009a, 2022, 2023). These preferences for jet modes may derive from mechanical limitations or performance targets provided by different vortex ring flows.

In contrast to many jet-propelled animals such as salps, medusozoans, and siphonophores, cuttlefishes (another cephalopod related to squids) have rigid bodies, skirtlike fins, and benthic lifestyles. With an internal cuttlebone made of calcium carbonate, cuttlefish are able to maintain neutral buoyancy but are limited in body flexibility (Denton and Gilpin-Brown, 1961; Hanlon and Messenger, 1996; Hanlon *et al.*, 2018). In general, animals with flexible bodies are considered more maneuverable (smaller turning radii) than animals with rigid bodies because they achieve greater body curvature and have lower moments of inertia (Fish, 1999; Walker, 2000; Parson *et al.*, 2011). However, some rigid-bodied animals such as beetles, cuttlefishes, and turtles are notable exceptions and can turn with low length-specific turning radii (Fish and Nicastro, 2003; Rivera *et al.*, 2006; Jastrebsky *et al.*, 2016). In addition to their rigid body structure, cuttlefish have long skirtlike fins surrounding the mantle that together with the jet contribute to propulsion, setting them apart from salps, medusozoans, and siphonophores, which rely exclusively on jet propulsion (Kier, 1989; Hanlon and Messenger, 1996; Jereb and Roper, 2005; Guerra, 2006; Hanlon *et al.*, 2018). In contrast to more pelagic jetters, cuttlefish are also relatively benthic animals, living in reef systems, where precise, controlled movements are advantageous for navigating complex structure.

Little is known about the turning capabilities of most cuttlefishes. Based on kinematic measurements, adult dwarf cuttlefish (*Sepia bandensis*) are among the tightest-turning animals in the oceans, outperforming both rigid and most soft-bodied animals (Jastrebsky *et al.*, 2016). Agility (angular velocity) in *S. bandensis* is more moderate, with flexible-bodied animals of similar size turning an order of magnitude faster (Jastrebsky *et al.*, 2016). In hatchling cuttlefish, there are species-specific differences in turning abilities. *Sepia officinalis* hatchlings turn faster (maximum angular velocity, $\Omega_{max} = 250° \text{ s}^{-1}$) than *S. bandensis* hatchlings ($\Omega_{max} = 89° \text{ s}^{-1}$), but both species turn with similar tightness (minimum length-specific turning radius of a turn, $(R/L)_{min} \sim 0.024$) (Ganley *et al.*, 2024). Faster turns in *S. officinalis* hatchlings are driven by higher jet velocities and angular impulses but smaller L_ω/D_ω than *S. bandensis* (Ganley *et al.*, 2024). Both species favor short, repetitive jets over longer jet flows to perform turns (Ganley *et al.*, 2024). Although kinematic data of adult cuttlefish and flow quantification data of hatchling cuttlefish are

available, nothing is known about jet or fin flows during turning in adult cuttlefish or how different hydrodynamic properties in adult cuttlefish correlate with kinematic parameters.

In this study, an integrated kinematic/hydrodynamic analysis was used to quantify the turning ability of adult *S. bandensis*. Three hypotheses were examined. (1) Adult *S. bandensis* will use shorter, lower-velocity jets for tight turns and longer, higher-velocity jets for fast turns. Although jet length and jet velocity ranges of adult cuttlefish were expected to be lower than those reported for adult squid because of cuttlefish's slower swimming speed, relatively smaller mantle volume, and greater reliance on the fins for propulsion, a trend toward longer, higher-velocity jets for high-angular-velocity turns, similar to patterns reported in squid, was predicted. (2) Orientation will play a more reduced role in turning than observed in squid. This prediction was based on a greater need (relative to more pelagic squids) to turn with similar proficiency across orientations when navigating complex reef environments, where forward/backward movements are common (Hanlon and Messenger, 1996; Hanlon *et al.*, 2018). (3) *Sepia bandensis* will rely more heavily on jet mode I and lower jet velocities than squids to achieve turns. This prediction was based on cuttlefish's preference for slower overall swimming speeds and residence in more benthic, complex habitats where short, low-velocity pulses are useful for maneuvering in tight spaces (Hanlon and Messenger, 1996; Hanlon *et al.*, 2018). In summary, this study aims to quantify the turning abilities of adult cuttlefish *S. bandensis* using both kinematic and hydrodynamic analyses.

Materials and Methods

Study animal

Eight juvenile/adult *Sepia bandensis* Adam, 1939 (total length [L] = 7.38 ± 1.48 cm) were purchased from the Marine Biological Laboratory in Woods Hole, Massachusetts, and shipped to Old Dominion University in Norfolk, Virginia, for experiments. Individuals were kept in mesh-lined 5-gal buckets suspended within a 450-gal recirculating tank (30 ppt, 26.5 °C). Holes were drilled in the 5-gal buckets to facilitate water flow through the mesh lining, and pool noodles were affixed to the bucket rims to provide buoyancy. Animals were fed fresh and frozen *Mysid* spp. as well as live *Palaemonetes* spp. All research was conducted under Institutional Animal Care and Use Committee protocol 21-002.

Data collection

For experimental trials, an animal was placed in a 10-gal glass aquarium filled with filtered seawater matching the salinity and temperature of the holding tanks and seeded with light-reflective particles (polyamide, 50 μm; Dantec Dynamics, Skövlunde, Denmark). A TSI V3V-8000 probe (three 2048 × 2048-pixel cameras, 14 × 14 × 10-cm sampling volume; TSI, Shoreview, MN) was used to capture paired images of particles in three dimensions for flow field measurements. A dual-pulsed laser (EverGreen HP, 340 mJ, 532 nm, 15 Hz, Δt = 2000 μs; Lumibird, Bozeman, MT) synchronized to the probe using TSI hardware and V3V 4G software was used to illuminate a cylindrical volume of particles. In addition to the flow quantification camera, three Falcon cameras (1400 × 1024 pixels, 100 frames s^{-1}; Teledyne Dalsa, Waterloo, Ontario) were positioned around the tank to capture dorsal (one camera) and lateral (two cameras) views of the cuttlefish turning in the tank (Fig. 1). Timing and synchronization of the three cameras comprising the V3V-8000 probe were achieved using TSI's Insight 4G software and synchronizer hardware. Video acquisition, timing, and synchronization of the three Falcon cameras were achieved using a DVR Express Core2 system and CoreView Software (IO Industries, London, Ontario). Image acquisition for the V3V-8000 and Falcon cameras was initiated simultaneously, with video time stamps used to correlate frames from the V3V-8000 probe (7.5 Hz) with those of the Falcon cameras (100 Hz). Halogen lights with red (>600-nm) filters were used for illumination of video frames captured from the Falcon cameras. Additional filters were used with the Falcon cameras and TSI probe to eliminate cross illumination from the different light sources, that

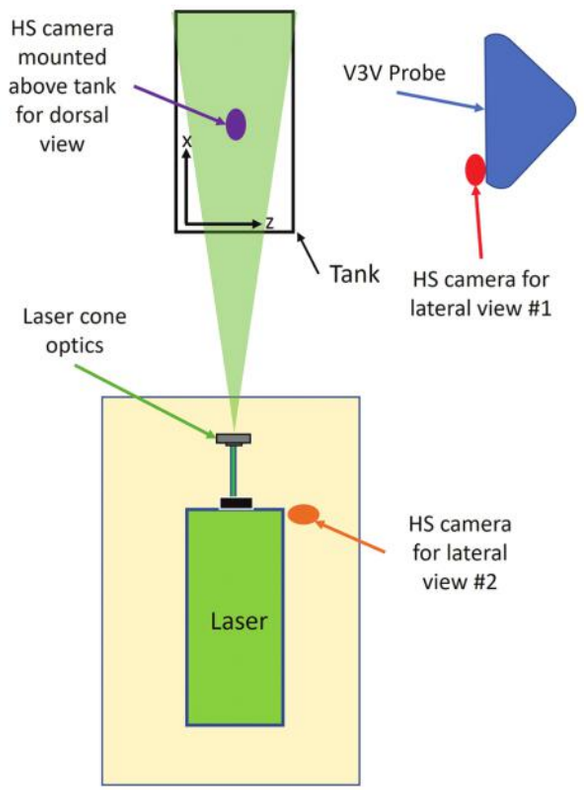

Figure 1. Experimental setup for cuttlefish (*Sepia bandensis*) turning study. The positions of high-speed (HS) cameras, 3D probe, and laser are depicted. Not to scale.

is, green-wavelength laser and red-wavelength halogen. Calibration of the V3V-8000 probe was achieved by collecting images of an illuminated grid at 5-mm intervals through the working volume and performing a dewarping procedure within TSI Insight 4G. Calibration of the Falcon cameras was achieved by collecting images of rulers affixed to a plexiglass box and determining the pixel-to-centimeter ratio in ImageJ (National Institutes of Health, Bethesda, MD).

Prior to data collection, individuals were allowed to acclimate in the viewing tank for 5–10 min. A data collection "run" lasted 40 s, with 300 paired images from the V3V-8000 probe and 4000 images from each Falcon camera being collected over the run. To reduce stress on the animals, 3–10-min breaks were provided between runs, and a maximum of 35 runs per animal were performed in a day. Cuttlefish that spent an inordinate amount of time on the edges of the tank and outside the sampling volume were encouraged into the center of the tank using a net. However, all turns used for analysis were spontaneous without interference from the net.

Data analysis

Kinematic analysis. Turns were identified using the following three criteria: (1) the animal had to exhibit a change in heading of >9°, (2) the cuttlefish had to turn primarily in the *x-z* plane, and (3) the turn had to be visible in both the dorsal view and at least one of the lateral views. Landmarks on the animal's body (seven points in dorsal view, six points in lateral view) were then digitized using motion-tracking software (Hedrick, 2008; Fig. 2A, B). Cross-validation criteria or mean-squared error techniques were used to smooth

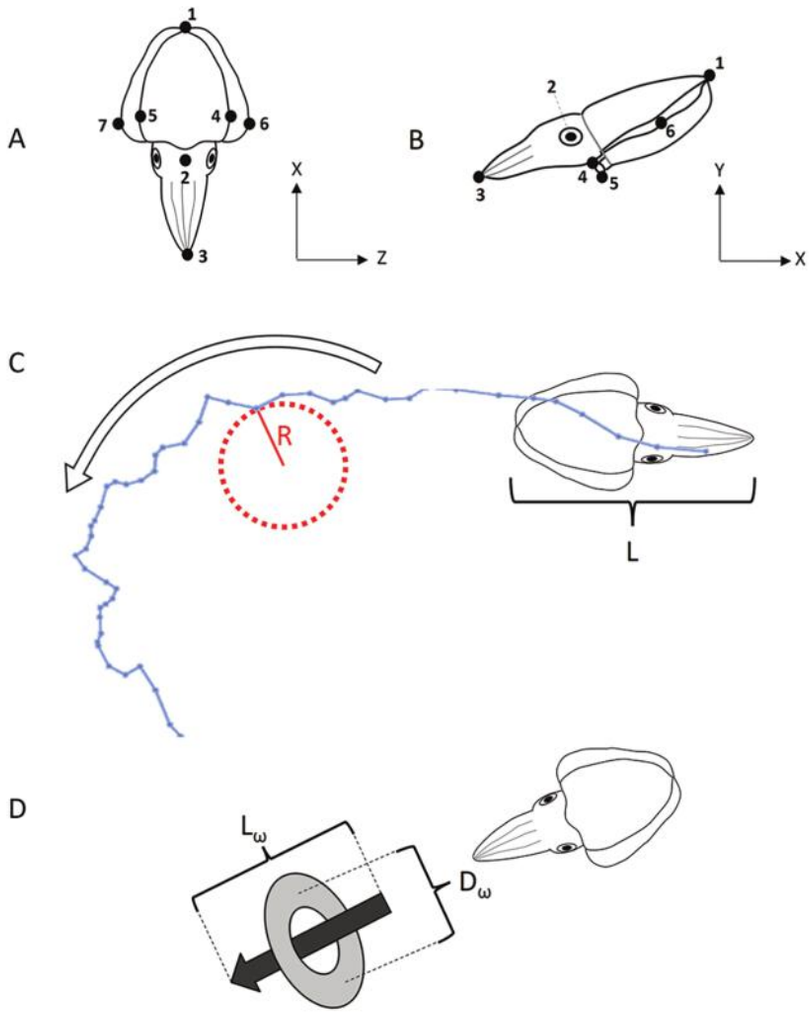

Figure 2. Illustration of methods for measuring *Sepia bandensis* turning. (A) Points for body tracking in the dorsal view. (B) Points for body tracking in the lateral view. (C) Illustration from a turn in which the center of rotation (COR) points are overlaid in blue. The radius (R) of the COR path was measured throughout the turn, averaged, and divided by total length (L) of the animal to compute a length-specific radius (R/L). The white arrow depicts the direction of the turn. (D) Stylized representation of jet length (L_ω) and diameter (D_ω) measures.

data before kinematic measures were calculated (Walker, 1998). The tracked points were used to calculate the average angular velocity (Ω_{ave}) throughout the turn and Ω_{max} during the turn. To control for outliers and tracking error, the top 10% of values of angular velocity were removed to determine Ω_{max} for each turn. Angular velocity is defined as the rate of change of the angular orientation of the cuttlefish in the *x*-*z* plane. The points used to determine angular velocity were the tail tip and forwardmost arm tip, as the cuttlefish is assumed to turn as a rigid body. This is visually verified in the data for the animal centerline, as expected given the rigid structure of the cuttlebone. The motion of animal extremities (such as fins) is not directly relevant to measuring the rate of turn of the animal body as a whole. The center of rotation (COR) was calculated between each frame using tracked points to determine the point in the dorsal view that moved the least during the turn. The radius of curvature of the COR (R) was calculated using

$$\frac{1}{R} = \frac{z''}{[1 + (z')^2]^{3/2}}, \tag{1}$$

where $z' = dz/dx = \dot{z}/\dot{x}, z'' = d^2z/dx^2 = (\dot{x}\ddot{z} - \dot{z}\ddot{x})/\dot{x}^3$, x and z are the coordinates of the COR in the dorsal view, t is time, the overdot represents time differentiation, and the derivatives were evaluated using fourth-order accurate finite difference equations (Fig. 2C). The COR was not restricted to the body of the animal. Instead, it could lie along a line at a fixed angle (α) with respect to the tracked body segment, where α and the position of the COR along the line at this angle were selected so that the movement of the COR during the turn was minimized. Mean R of each turn sequence was calculated. To control for outliers and errors in tracking, the bottom 10% of R values were removed for each sequence to determine the minimum radius of a turn (R_{min}). All R values were standardized for animal length (L) to control for size differences, resulting in measures of mean length-specific turning radius ($(R/L)_{mean}$ and $(R/L)_{min}$).

Hydrodynamic analysis. Defocusing digital particle tracking velocimetry (DDPTV) was used to quantify flow fields around turning cuttlefish. Details on processing parameters can be found in Bartol *et al.* (2016, 2018, 2022, 2023). In general, 10,000–25,000 (some up to 70,000) velocity vectors were found per image pair using a 16-mm voxel, 75% voxel overlap, and smoothing factor of 1, which assigns a greater weight to particles near the voxel center to smooth the velocity field. Readers can refer to the following papers for additional details about the DDPTV technique and error analyses associated with the approach: Pereira *et al.* (2000, 2006), Troolin and Longmire (2009), and Couch and Krueger (2011). For flow fields to be included in the study, flow features associated with the turn had to be completely enclosed within the sampling volume and away from boundary edges. If a jet pulse was visible for multiple frames, the frame where vorticity had completely separated from the cuttlefish body and where impulse and angular impulse were maximal was processed. For sequences with more than one jet pulse, the jet pulse with the highest impulse and angular impulse was analyzed, provided it was spatially separated from other jet-generated vortices. Not all turns meeting the kinematic criteria above included resolvable propulsive flows, as vortex structures were sometimes out of or near the edge of the sampling volume. Since these sequences did not meet the criteria above, they were not analyzed. To reduce erroneous vectors associated with the illuminated body, the body of the animal was removed with the polygon mask feature in TSI's V3V 4G software, whereby the vertices of the polygon were defined by mouse clicks along the contours of the cuttlefish body. All velocity/vorticity figures were produced in Tecplot 360 (Bellevue, WA). Average jet velocity (U_{jave}), maximum jet velocity (U_{jmax}), jet length (L_ω), jet diameter (D_ω), jet impulse ($\mathbf{I}$), and jet angular impulse ($\mathbf{A}$) were calculated using an in-house MATLAB routine. Jet diameter was the distance between jet vorticity cores (defined as regions >90% of peak jet vorticity) perpendicular to the jet centerline (Fig. 2D). Jet length was the extent over which the jet vorticity field (perpendicular to D_ω) was over a specified threshold (20% of the maximum vorticity; Fig. 2D). Linear impulse was calculated using the following equation:

$$\frac{\mathbf{I}}{\rho} = \frac{1}{2}\int_{jet} \mathbf{x} \times \boldsymbol{\omega} dV, \tag{2}$$

where $\mathbf{x}$ is the position vector and $\boldsymbol{\omega}$ is the vorticity vector ($\boldsymbol{\omega} = \nabla \times \mathbf{u}$, where $\mathbf{u}$ is the velocity vector and the partial derivatives were calculated using central differences), ρ is the fluid density, and the integral is computed over the volume of the vortex, V, where the vorticity is nonzero (Saffman, 1995). Angular impulse was calculated using the following equation derived from Wu *et al.* (2007):

$$\frac{\mathbf{A}}{\rho} = -\frac{1}{2}\int |\mathbf{x}|^2 \boldsymbol{\omega} dV. \tag{3}$$

By default, $\mathbf{A}$ associated with a vortex selected for analysis was computed with respect to the centroid of the vorticity magnitude of the vortex using the above equation. The origin of the position vector $\mathbf{x}$ in equations (2) and (3) is arbitrary, but for purposes of calculation, the centroid of vorticity of the selected vortex is used for the initial calculations. To determine $\mathbf{A}$ about the center of mass of the cuttlefish, the origin of the calculated impulse was shifted (by moving the origin of $\mathbf{x}$) to the cuttlefish center of mass using the distance between the center of mass of the animal and the centroid of the vortex (determined from the custom MATLAB routines) in accordance with equation (3). Given that cuttlefish were primarily turning in the *x*-*z* plane, $\mathbf{A_{yaw}}$ was the focus of this study, although $\mathbf{A_{pitch}}$ and $\mathbf{A_{roll}}$ were also measured.

Statistics

Statistics were done in SPSS (ver. 28.0.0; IBM). All variables failed Shapiro-Wilks significance testing and required transformation. Most variables were $\log_{10}$ transformed to fit assumptions. However, Ω_{max} and L_ω/D_ω failed normality testing with $\log_{10}$ transformations and were instead transformed using the appropriate lambda from Tukey's ladder transformations. The absolute value of angular impulses for yaw, roll, and pitch were used for analysis, as magnitude, regardless of direction, was of interest. A three-way MANOVA was performed on transformed kinematic data to test for differences in test animal, turn orientation, and dataset. Dataset denotes whether the turn had associated resolvable hydrodynamic data. This variable was considered to test for bias in kinematic metrics when the added requirement of resolvable flow data within the sampling volume is used. A separate two-way MANOVA was completed on transformed flow field data to test for differences in test animal and turn orientation. The Pillai's trace statistic was used to determine significance, as suggested for uneven group sizes. Follow-up ANOVAs and Tukey *post hoc* tests were performed when necessary (*e.g.*, test subjects) to determine where significance occurred. Linear regressions were performed on untransformed data. All means are reported ±SEM unless otherwise stated. Significance was determined using $\alpha \leq 0.05$.

Results

A total of 186 turns from eight individuals were considered for kinematic analysis; 47 of these turns included resolvable 3D velocimetry data that fell within the sampling volume and were considered further for hydrodynamic analysis. One cuttlefish (L = 5.2 cm) did not produce resolvable 3D velocimetry data and thus was considered only for kinematic analyses. Of the 186 total turns, 72.6% were performed in an arms-first orientation, and 27.4% were performed in a tail-first orientation.

Kinematic variables

The average displacement of the animal in the y-direction was 0.25 ± 0.27 body lengths, confirming that turns were primarily in the x-z plane. The $(R/L)_{mean}$ across all cuttlefish was 0.14 ± 0.013, with a range of 0.0107–1.16; the $(R/L)_{min}$ was 0.013 ± 0.002, with a range of 0.00036–0.20. The Ω_{ave} of turns was 45.85° ± 2.70° s^{-1}, with a range of 5.53°–254.77° s^{-1}. The Ω_{max} reached during turning was 110.34° ± 7.09° s^{-1}, with a range of 24.97°–910.49° s^{-1}. In addition, there was a significant positive relationship between Ω_{ave} and $(R/L)_{mean}$ (linear regression, $F_{1, 185}$ = 24.61, P < 0.001; R^2 = 0.118; Fig. 3A), as well as a significant positive relationship between Ω_{max} and $(R/L)_{min}$ for all turns (linear regression, $F_{1, 185}$ = 115.97, P < 0.001; R^2 = 0.386; Fig. 3B).

When kinematic variables were analyzed, both test animal (MANOVA, $F_{28, 632}$ = 1.838, P = 0.006) and dataset type (*i.e.*, kinematic only *vs.* kinematic + hydrodynamic) were significant (MANOVA, $F_{4, 155}$ = 3.547, P = 0.008). Orientation was not significant (MANOVA, $F_{4, 155}$ = 1.190, P = 0.318), and there were no significant interaction factors (Table 1). Follow-up ANOVAs on test animals showed that individuals had significantly different $(R/L)_{mean}$ values (ANOVA, $F_{7, 186}$ = 5.770, P < 0.001) and $(R/L)_{min}$ values (ANOVA, $F_{7, 186}$ = 5.155, P < 0.001). When individuals were examined more closely, four cuttlefish turned more tightly than the other four cuttlefish (Fig. 4A, B). While not significant, it is interesting that the cuttlefish that turned the fastest (ID 8; Ω_{ave} = 72.23; Ω_{max} = 193.31° s^{-1}) also produced the widest turns ($(R/L)_{mean}$ = 0.381; $(R/L)_{min}$ = 0.042; Fig. 4). No significant difference in Ω_{ave} (ANOVA, $F_{7, 186}$ = 0.994, P = 0.438) or Ω_{max} (ANOVA, $F_{7, 186}$ = 0.994, P = 0.438) was detected among individuals (Fig. 4C, D). Interestingly, Ω_{ave} (ANOVA, $F_{1, 186}$ = 10.360, P = 0.002) and Ω_{max} (ANOVA, $F_{1, 186}$ = 9.238, P = 0.003) were significantly lower for sequences with accompanying flow fields than those without, but no differences were detected for either $(R/L)_{mean}$ (ANOVA, $F_{1, 186}$ = 0.091, P = 0.400) or $(R/L)_{min}$ (ANOVA, $F_{1, 186}$ = 0.012, P = 0.817). For sequences with flow fields, Ω_{ave} and Ω_{max} were 32.34° ± 2.27° s^{-1} and 82.42° ± 5.79° s^{-1}, respectively; Ω_{ave} and Ω_{max} for sequences without resolvable flow fields were 50.55° ± 3.47° s^{-1} and 120.1° ± 9.21° s^{-1}, respectively (Fig. 5A, B).

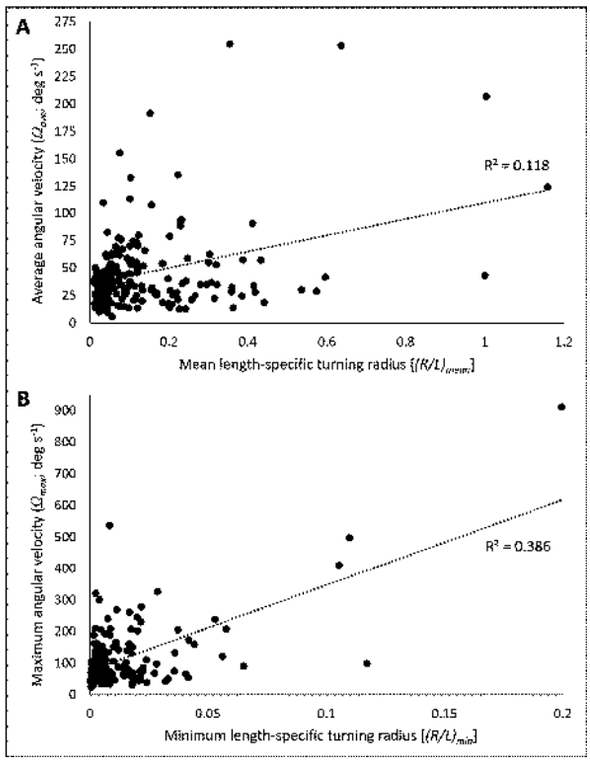

Figure 3. Regressions between angular velocity and turn radius for turns completed by *Sepia bandensis*. (A) Linear relationship between average angular velocity (Ω_{ave}) and mean length-specific turning radius ($(R/L)_{mean}$). (B) Linear relationship between maximum angular velocity (Ω_{max}) and minimum length-specific turning radius ($(R/L)_{min}$). Significant regressions include trend lines and R^2 values.

Table 1

Three-way MANOVA results for kinematic data

Variable	*F*	df	*P*
Orientation	1.190	4, 155	0.318
Individual	1.838	28, 632	0.006*
Dataset	3.547	4, 155	0.008*
Orientation × individual	1.303	28, 632	0.138
Orientation × dataset	2.135	4, 155	0.079
Individual × dataset	1.465	24, 632	0.071
Orientation × individual × dataset	1.352	16, 632	0.160

Note: The three factors were orientation (arms-first *vs.* tail-first), individual (squid test subject), and dataset (kinematic data only *vs.* kinematic data with accompanying flow data). Four dependent variables were considered: (1) average angular velocity, (2) maximum angular velocity, (3) average length-specific turning radii, and (4) minimum length-specific turning radii. The multiplication symbols indicate interaction effects, and the asterisks denote statistical significance of $P < 0.05$.

Hydrodynamic variables

Adult *Sepia bandensis* produced jets with a wide range of hydrodynamic signatures, including both jet mode I and jet mode II. Some jets had complex vorticity fields, such as multiple discrete rings, interconnected vortex rings, and elongated vorticity structures with vortex ring elements (Fig. 6). Although jet mode II and other modes were observed in some turning sequences, jet mode I was most prevalent, with short vortex rings sometimes being produced in succession (Fig. 7). The U_{jave} was 14.11 ± 1.81 cm s^{-1} (range = 1.90–66.84 cm s^{-1}), and the U_{jmax} was 21.92 ± 2.57 cm s^{-1} (range = 3.28–91.75 cm s^{-1}). The average L_ω/D_ω for turning jets was 2.47 ± 0.18, with a range of 1.09–6.56.

When hydrodynamic variables were analyzed, test animal was significant (MANOVA, $F_{60, 186} = 1.663$, $P = 0.005$), but turning orientation (MANOVA, $F_{10, 26} = 1.220$, $P = 0.324$) and the interaction factor (MANOVA, $F_{40, 116} = 0.875$, $P = 0.680$) were not. Follow-up ANOVAs indicated that there were significant differences in U_{jave} (ANOVA, $F_{6, 186} = 6.237$, $P < 0.001$) and U_{jmax} (ANOVA, $F_{6, 186} = 5.376$, $P < 0.001$) among individuals (Fig. 8A, B).

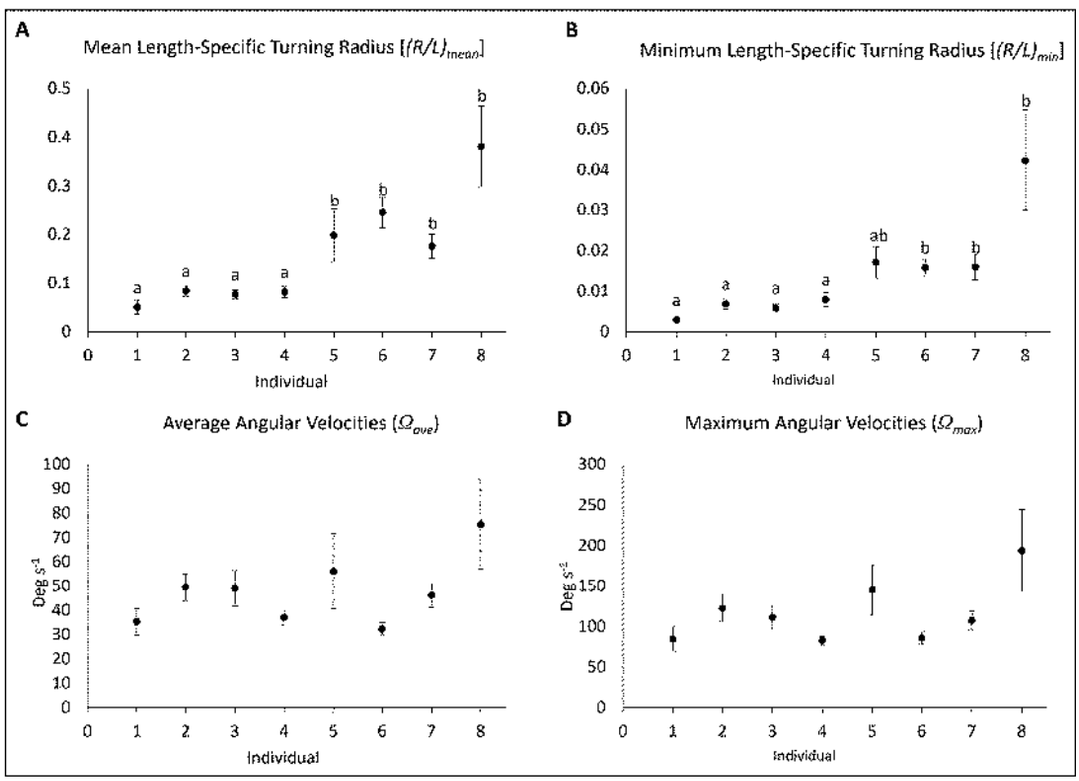

Figure 4. Individual-level difference in kinematic turning measures for *Sepia bandensis*. (A) Mean length-specific turning radius ($(R/L)_{\text{mean}}$) for each individual cuttlefish. (B) Average minimum length-specific turning radius ($(R/L)_{\text{min}}$) for each individual cuttlefish. (C) Average angular velocity (Ω_{ave}) of turns performed by individuals. (D) Average maximum angular velocity (Ω_{max}) performed by individuals. Individual ID number is consistent throughout the figure and across figures, and all error bars are SEM. Significance is denoted by different lowercase letters; no significance was found in (C, D).

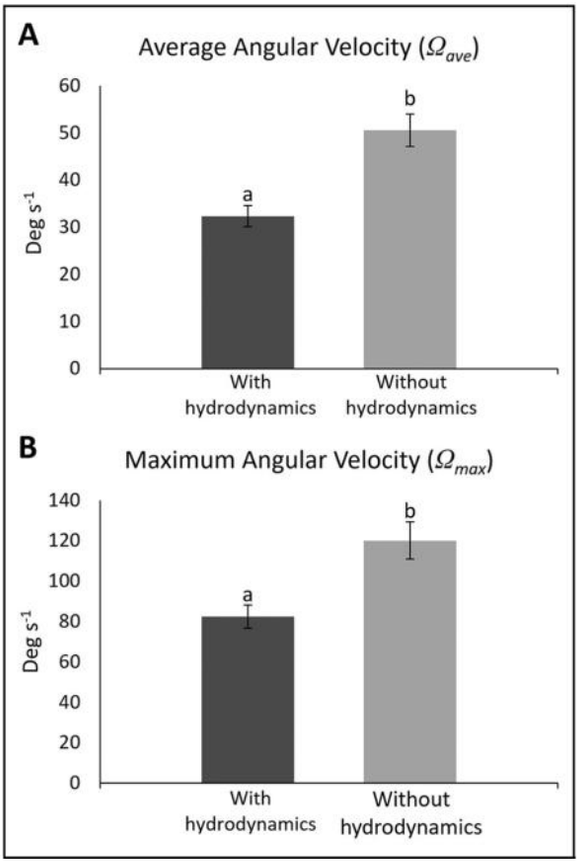

Figure 5. Kinematic measures between datasets of turning *Sepia bandensis*. (A) Average angular velocity (Ω_{ave}) of sequences with accompanying resolvable hydrodynamic data and without. (B) Average maximum angular velocity (Ω_{max}) of sequences with accompanying resolvable hydrodynamic data and without. Error bars are SEM, and significance is denoted with different lowercase letters.

The cuttlefish with the tightest turning capacity (ID 1; $(R/L)_{min} = 0.0013$) produced some of the lowest jet velocities ($U_{jave} = 2.74$ cm s^{-1}; $U_{jmax} = 4.80$ cm s^{-1}) and angular velocities ($\Omega_{ave} = 35.15°$ s^{-1}; $\Omega_{max} = 84.33°$ s^{-1}; Figs. 4, 8). One cuttlefish (ID 3) produced the highest U_{jave} (~32 cm s^{-1}) and a trend toward the highest U_{jmax} (~48 cm s^{-1}; Fig. 8). There was no significant difference in the L_ω/D_ω across individuals (ANOVA, $F_{6,186} = 0.940$, $P = 0.479$). Linear regressions of L_ω/D_ω and angular velocity (Ω_{ave}, $F_{1,46} = 0.0176$, $P = 0.677$; Ω_{max}, $F_{1,46} = 1.606$, $P = 0.212$) and of L_ω/D_ω and turning radius ($(R/L)_{mean}$, $F_{1,46} = 0.655$, $P = 0.423$; $(R/L)_{min}$, $F_{1,46} = 0.360$, $P = 0.552$) were not significant. Furthermore, linear regressions of jet velocity and turn tightness were insignificant for both average values (U_{jave} *vs.* $(R/L)_{mean}$, $F_{1,46} = 2.127$, $P = 0.152$) and extreme values (U_{jmax} *vs.* $(R/L)_{min}$, $F_{1,46} = 0.687$, $P = 0.412$). A linear regression of jet velocity and angular velocity was also insignificant (U_{jave} *vs.* Ω_{ave}, $F_{1,46} = 1.597$, $P = 0.213$).

There were no significant differences in $\mathbf{A_{yaw}}$, $\mathbf{A_{roll}}$, and $\mathbf{A_{pitch}}$ between individuals; $\mathbf{A_{yaw}}$ was 1.5–2 times higher than $\mathbf{A_{roll}}$ and $\mathbf{A_{pitch}}$, and there was a greater range of $\mathbf{A_{yaw}}$ than either $\mathbf{A_{roll}}$ or $\mathbf{A_{pitch}}$. See Table 2 for a list of values.

Discussion

This study examined the turning abilities of adult cuttlefish, *Sepia bandensis*. Using kinematic and hydrodynamic analyses, 186 turns from eight individuals were recorded and analyzed to test three main hypotheses: (1) adult *S. bandensis* will favor short, low-velocity jets to complete tight turns while using long, fast jets for quick turns; (2) adult cuttlefish will be equally proficient at turning in the arms-first and tail-first orientation; and (3) slower jet velocities and jets with discrete vortex rings (known as jet mode I) will be used more frequently by adult *S. bandensis* compared to previously studied squid species.

Relationships between turning kinematics and jet flows

In this study, an integrated kinematic and hydrodynamic analysis was used to quantify the turning ability of adult *S. bandensis*. The observed turning radii of *S. bandensis* ($(R/L)_{mean}$ ~ 0.14; $(R/L)_{min}$ ~ 0.013) are similar to tight-turning squids ($(R/L)_{mean}$ ~ 0.15–0.20; $(R/L)_{min}$ ~ 0.006–0.020) (Bartol *et al.*, 2022, 2023; Ganley *et al.*, 2023). While Jastrebsky *et al.* (2016) reported lower turning radii ($(R/L)_{mean}$ ~ 0.095; $(R/L)_{min}$ ~ 0.001) for *S. bandensis*, this may be a product of turns being induced by prey targets, which potentially promotes tighter turns as animals maintain alignment with moving prey. Interestingly, the lowest $(R/L)_{min}$ value was similar across both studies (Jastrebsky *et al.*, 2016: 0.00013; this study: 0.00036). Tight turning is important for navigation in complex environments, such as reef systems where *S. bandensis* often resides, and for making fine adjustments for crypsis, which is critical for prey capture and predator avoidance (Hanlon and Messenger, 1996; Hanlon *et al.*, 2018).

Sepia bandensis demonstrated angular velocities (Ω_{ave} ~ 46° s^{-1}; Ω_{max} ~ 110° s^{-1}) in this study that were in reasonable agreement with those reported in previous studies for the dwarf cuttlefish *S. bandensis* (Ω_{ave} ~ 55° s^{-1}; Ω_{max} ~ 160° s^{-1}), longfin squid *Doryteuthis pealeii* (Ω_{ave} ~ 27°–38° s^{-1}; Ω_{max} ~ 73°–82° s^{-1}), and shortfin squid *Illex illecebrosus* (Ω_{ave} ~ 27°–46° s^{-1}; Ω_{max} ~ 70°–108° s^{-1}), though values of Ω for this study are lower than for Atlantic brief squid *Lolliguncula brevis* (Ω_{ave} ~ 70°–110° s^{-1}; Ω_{max} ~ 140°–268° s^{-1}) (Jastrebsky *et al.*, 2016; Bartol *et al.*, 2022, 2023; Ganley *et al.*, 2023). Given their small size (low rotational resistance) and heavy reliance on escape jetting, it seems reasonable that *L. brevis* would display high angular velocities (Hanlon *et al.*, 1983; Finke *et al.*, 1996; Good *et al.*, 2023). Interestingly, the highest Ω_{max} recorded in this study (910.5° s^{-1}) was significantly larger than that recorded previously for cuttlefish (485° s^{-1}; Jastrebsky *et al.*, 2016) or squid (775° s^{-1}; Bartol *et al.*, 2022). Therefore,

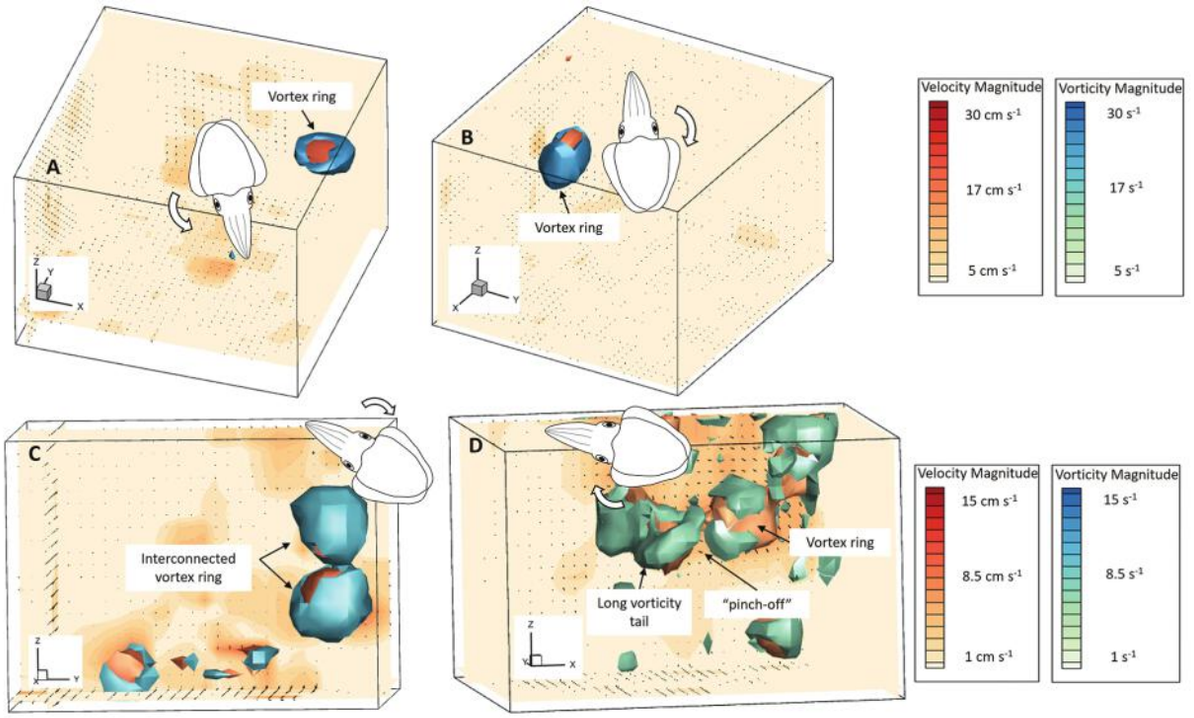

Figure 6. Examples of 3D velocity and 3D vorticity fluid flow produced by *Sepia bandensis* during turning. Velocity isosurfaces are shown in warm colors (orange/red), and vorticity isosurfaces are shown in cool colors (blue/green). The cartoon illustrates the approximate location of the cuttlefish during the turn (not to scale). (A) Arms-first counterclockwise turn with a resulting single vortex ring. (B) Tail-first clockwise turn with a resulting single, slightly elongated vortex ring. (C) Tail-first clockwise turn with interconnected vortex rings. (D) Arms-first clockwise turn with a leading vortex ring and vorticity tail, which is pinched off from the ring. (A) and (B) are considered jet mode I, and (C) and (D) are jet mode II.

while *S. bandensis* does not routinely perform fast turns, it can reach high angular velocities when needed.

The first hypothesis of this study was not supported, as tighter turns were not associated with lower L_ω/D_ω, U_{jave}, and U_{jmax} and faster turns were not linked to higher L_ω/D_ω, U_{jave}, and U_{jmax}. Indeed, neither L_ω/D_ω nor U_{jave}/U_{jmax}, on their own, was a reliable predictor of agility (Ω) or maneuverability (R/L). Given that most jets were short ($L_\omega/D_\omega < 4$) and only one jet had an $L_\omega/D_\omega > 5$, it is not surprising that a strong relationship between L_ω/D_ω and either R/L or Ω was not found, as the spread of data was limited. However, the range of U_{jave} and U_{jmax} was significant, and thus the absence of a relationship between U_{jave}/U_{jmax} and Ω or between U_{jave}/U_{jmax} and R/L was unexpected. One confounding factor may be jet frequency, which was not measured in this study. In squids, Ω increases with jet frequency, and Ω is affected by multiple factors that include not only jet frequency but also U_{jave}, U_{jmax}, and L_ω/D_ω (Bartol *et al.*, 2023). A similar combination of factors may be at work in this study, making it difficult to isolate any one jet factor in turn performance.

Orientation

Although prior studies of squids have found differences in kinematic and hydrodynamic properties according to turn orientation (Bartol *et al.*, 2022, 2023), a consistent orientation effect was not found in cuttlefish, which provides support for the project's second hypothesis. In squids, such as *L. brevis* and *I. illecebrosus*, **I**, $\mathbf{A_{yaw}}$, U_{jave}, U_{jmax}, and L_ω/D_ω are greater during tail-first turns than arms-first turns, resulting in higher angular velocities but wider turning radii (Bartol *et al.*, 2022, 2023). Although R/L is lower for arms-first turns, and $\mathbf{A_{yaw}}$ and L_ω/D_ω are generally higher during tail-first turns in the squid *D. pealeii* as well, Ω_{ave} and Ω_{max} can be greater during arms-first turns when high-impulse, high-velocity jets are employed (Bartol *et al.*, 2022, 2023). For squids, turning tightly in the arms-first orientation is beneficial for steering through complex or uncertain environments, when aligning with prey targets, and during periods of high vigilance, all of which require fine corrections in heading. Alternatively, turning quickly in the tail-first orientation is important for escape, high-speed cruising, vertical migrations, and schooling, when sudden powerful course corrections are required (Bartol *et al.*, 2023). Cuttlefish have less need for a high-powered tail-first mode because they do not cruise at high speeds, undergo rapid vertical migrations, or school to the extent observed in squids (Hanlon and Messenger, 2018). Indeed, having the capacity to turn with equal proficiency in both orientations is well suited for a cuttlefish's lifestyle, whereby it engages in ambush-style hunting, maneuvers in complex habitats, and escapes from a multitude of predators within a densely populated reef community (Rizzari *et al.*, 2014; Catano *et al.*, 2015, 2016)—behaviors

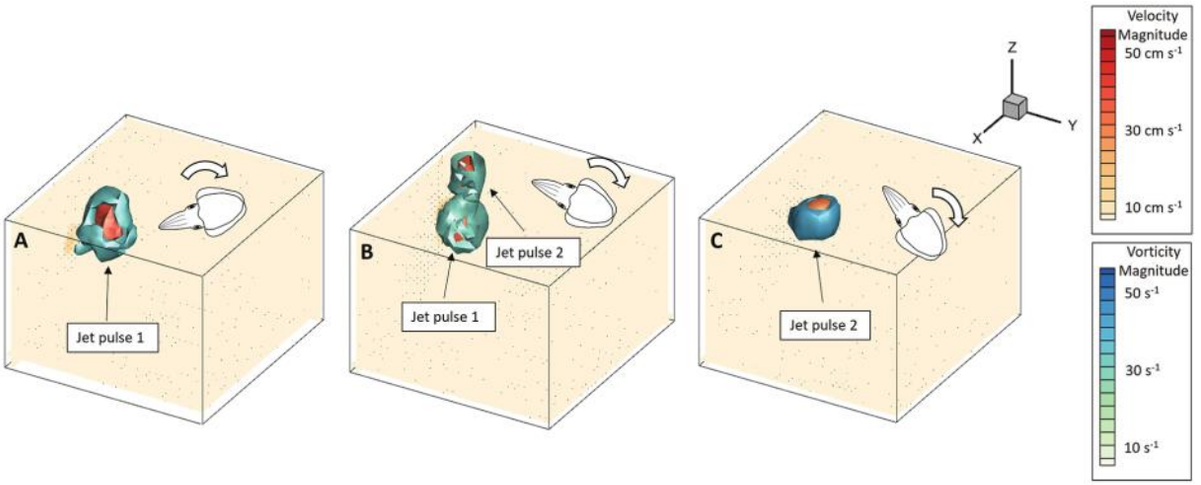

Figure 7. 3D velocity and vorticity isosurfaces produced by *Sepia bandensis* during a turn. Velocity isosurfaces are shown in warm colors (orange/red), and vorticity isosurfaces are shown in cool colors (blue/green). The cartoon illustrates the approximate location of the cuttlefish during the turn (not to scale). This turn was completed with an average angular velocity of ~50° s^{-1} and an average length-specific radius of 0.02. (A) $t = 0$ s. The first jet pulse in the turn produces an isolated vortex ring that powers the beginning of the clockwise tail-first turn. (B) $t = 0.13$ s. A second jet pulse produces another vortex ring to further rotate the animal. (C) $t = 0.27$ s. The first jet pulse moves out of the sampling volume, and the second jet pulse is visible.

that can all benefit from turning in either orientation. While squid must also hunt and escape, their hunting strategies tend more toward tail-first pursuits before reorienting for striking, and escape jetting is often not constrained as much by a complex habitat, therefore limiting the need for equal performance in both orientations. Furthermore, funnel muscle constraints are thought to contribute to orientation-based performance differences in squids (Bartol *et al.*, 2001, 2023; Kier and Thompson, 2003; Stewart *et al.*, 2010). Given the lack of significant orientation differences in kinematic or hydrodynamic properties, the radial and longitudinal funnel musculature of cuttlefish may differ from that of squids, perhaps providing greater force for funnel curvature and aperture control. This is an area of investigation worth exploring further, including an examination of turning and rectilinear swimming abilities together.

Jet characteristics

While *S. bandensis* produced a variety of jet wake signatures during turns, the predominant jet pattern was short ($L_\omega/D_\omega \sim 2.5$) vortex rings (jet mode I), sometimes in succession, with this pattern occurring in >85% of turns. This high reliance on jet mode I supports the project's third hypothesis. Because of the low number of jet mode II flows, it was not possible to accurately determine the transition of L_ω/D_ω between jet modes I and II, that is, *F*, or the physical limit of vortex formation (Gharib *et al.*, 1998; Krueger and Gharib, 2003). However, the observed mean L_ω/D_ω (~2.5) was below the *F* (3–4) reported for other cephalopods (Bartol *et al.*, 2016, 2022, 2023), which is consistent with the high prevalence of jet mode I. Hatchling *S. bandensis* and *Sepia officinalis* also show a preference for jet mode I during turns (76%–81%) (Ganley *et al.*, 2024). However, this heavy reliance on jet mode I differs from patterns observed in squids, such as *L. brevis*, *D. pealeii*, and *I. illecebrosus*, where a more balanced mix of jet modes I and II are employed during turns and where mean $L_\omega/D_\omega \geq 3.3$ (Bartol *et al.*, 2023). This difference may occur because the cuttlebone limits relative mantle volumes in cuttlefish, resulting in shorter overall jet pulses. Indeed, jet mode I is observed more often in adult *S. officinalis* (relative to squid) during rectilinear swimming as well (Gladman and Askew, 2023), providing support for this hypothesis. In rectilinear swimming, smaller jets can increase propulsive efficiency, while longer jets are used to maximize power and speed output (Bartol *et al.*, 2008, 2009a, b, 2016, 2022, 2023). Thus, greater reliance on jet mode I in cuttlefish may offer improved energy use during turns. Shorter, vectored jets also provide more controlled impulse throughout the turn path (Bartol *et al.*, 2022, 2023), and small jets are beneficial when sneaking up on prey or avoiding predators, because of a reduced flow signature compared to longer jets (*e.g.*, jet mode II).

The observed jet velocities ($U_{jave} \sim 14$ cm s^{-1}; $U_{jmax} \sim 22$ cm s^{-1}) are slightly higher than those recorded for some adult squids during turning maneuvers, such as *L. brevis* ($U_{jave} \sim 11$ cm s^{-1}; $U_{jmax} \sim 17$ cm s^{-1}) and *I. illecebrosus* ($U_{jave} \sim 10$ cm s^{-1}; $U_{jmax} \sim 15$ cm s^{-1}), but lower than those reported for other squids, such as *D. pealeii* ($U_{jave} \sim 38$ cm s^{-1}; $U_{jmax} \sim 62$ cm s^{-1}) (Bartol *et al.*, 2022, 2023). Along with heavy reliance on jet mode I, lower U_{jave} and U_{jmax} for cuttlefish was expected (third hypothesis) because cuttlefish swim slower and rely more heavily on their fins than do neritic squids (Hoar *et al.*, 1995). However, our data did not support this, with U_{jave} and U_{jmax} being fairly similar to those for *L. brevis* and *I.*

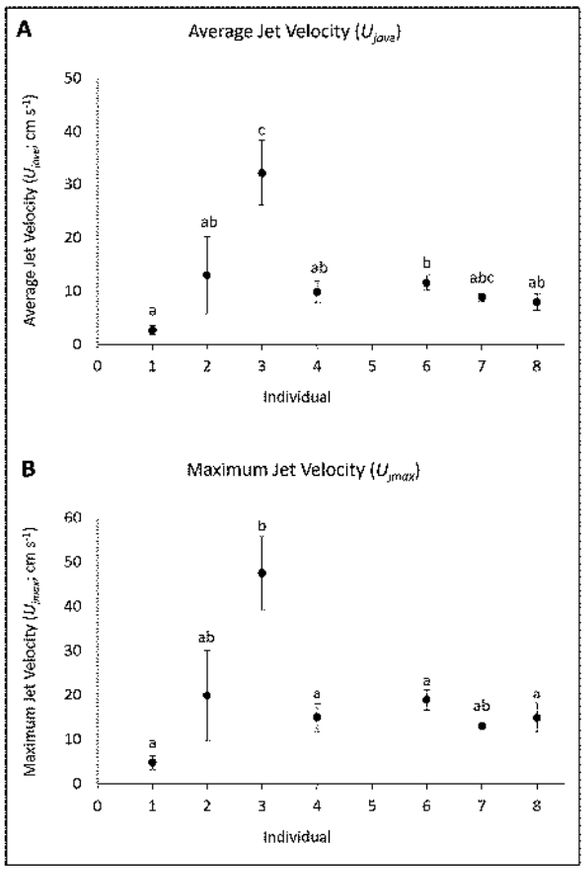

Figure 8. Jet velocities for individual *Sepia bandensis* during turns. (A) Average jet velocity (U_{jave}) for individuals. (B) Average maximum jet velocity (U_{jmax}) for individuals. Individual ID number is consistent throughout the figure and across figures. Note that individual ID 5 did not produce resolvable flows, that is, vortex structures fully within the sampling volume, and was excluded from hydrodynamic analyses. All error bars shown are SEM, and significance is denoted by different lowercase letters.

illecebrosus. Short but moderately fast jets are advantageous for turning, as they provide focused, repetitive impulse for sustaining and controlling rotation. In contrast to negatively buoyant squids, *S. bandensis* does not need to use its jet for buoyancy control. Rather, it can allocate more jet flow to **A** to effect the turn. The observed higher $\mathbf{A_{yaw}}$ relative to $\mathbf{A_{roll}}$ and $\mathbf{A_{pitch}}$ is not surprising given that the selected turns were performed primarily in the yaw plane. For the Atlantic brief squid *L. brevis*, the fins and arms play important roles in $\mathbf{A_{yaw}}$, $\mathbf{A_{roll}}$, and $\mathbf{A_{pitch}}$, contributing angular impulse to effect the turn, stability, and in the case of the arms reduced rotational resistance when they are pulled close to the body (Bartol *et al.*, 2022). Fin flows were not easily resolvable in this study because the fins were small (and transparent) and flows tended to stay close to the brightly lit body, making it difficult to track fin-induced particle fields. The role of the arms in turns was also not quantified. However, the fins were actively undulating during turns, and the arms were often curled or extended in a conical shape. Therefore, it is likely that both appendages contribute to turn performance, as is the case with squids. Subsequent studies incorporating flow quantification techniques that can isolate and track particles superimposed on the body would provide valuable insights on the role of the fins and arms of cuttlefishes during turns.

Kinematic-hydrodynamic relationships and methodological influences on measurements

The strong positive relationship between R/L and Ω was expected, given that this relationship has been documented in *S. bandensis* hatchlings (Ganley *et al.*, 2024) and in other taxa (Fish, 2002; Fish and Nicastro, 2003; Fish *et al.*, 2003, 2018; Maresh *et al.*, 2004; Rivera *et al.*, 2006; Parson *et al.*, 2011; Jastrebsky *et al.*, 2016; Sutherland *et al.*, 2019; Ganley *et al.*, 2023). This relationship has not been documented consistently in squids, however, possibly because of high behavioral variability (Jastrebsky *et al.*, 2016; Bartol *et al.*, 2022, 2023; Ganley *et al.*, 2023). Relative to hatchlings, where $(R/L)_{mean} = 0.67$ and $\Omega_{ave} = 38° \text{ s}^{-1}$ (Ganley *et al.*, 2024), adult *S. bandensis* in this study turned more tightly (lower R/L) and more quickly (higher Ω). Lower Ω for hatchlings is surprising, given that smaller animals generally have lower moments of inertia and higher Ω than do larger swimmers (Fish *et al.*, 2018; Fish and Holzman, 2019). Greater agility, that is, higher Ω, and greater maneuverability, that is, lower R/L, in adults relative to hatchlings may derive from greater muscle development, increased neural control, and more developed fins, which occur at older life stages (Thompson and Kier, 2001, 2006; Kier and Thompson, 2003; Dickel *et al.*, 2006; Kobayashi *et al.*, 2013; Liu *et al.*, 2017).

There were differences in turning performance among individual *S. bandensis*, with two main groups identified in this study: one group (individuals 1–4) that turned with $(R/L)_{mean} < 0.10$ and another group (individuals 5–8) that turned with $(R/L)_{mean} > 0.15$, including one cuttlefish (ID 8) that exclusively turned broadly with high angular velocity. Aside from this extremely fast and broad-turning individual, most cuttlefish had $\Omega_{max} = 75°–150° \text{ s}^{-1}$, reflecting their preference for relatively slow routine turns. This makes sense when viewed with an ecological lens, as slow, tight turns are necessary for routine behaviors, such as

Table 2

Summary of directional angular impulse results

Variable	Average (kg m^2 s^{-1})	Minimum (kg m^2 s^{-1})	Maximum (kg m^2 s^{-1})
$\mathbf{A_{yaw}}$	$4.88 \times 10^{-3} \pm 1.02 \times 10^{-3}$	2.55×10^{-4}	4.18×10^{-2}
$\mathbf{A_{roll}}$	$2.48 \times 10^{-3} \pm 4.08 \times 10^{-4}$	8.44×10^{-5}	9.50×10^{-3}
$\mathbf{A_{pitch}}$	$2.98 \times 10^{-3} \pm 4.62 \times 10^{-4}$	3.15×10^{-5}	1.35×10^{-2}

Note: No significant differences were found for individual, orientation, or dataset. **A**, angular impulse of jet.

Table 3

Compiled turning metrics for different taxa

Species	Common name	Average $(R/L)_{mean}$	Average $(R/L)_{min}$	Minimum $(R/L)_{min}$	Average Ω_{ave} (° s^{-1})	Average Ω_{max} (° s^{-1})	Maximum Ω_{max} (° s^{-1})	Study
Lolliguncula brevis[a]	Atlantic brief squid	0.009	0.0034	0.00042	110.3	268.4	725.8	Jastrebsky *et al.*, 2016
Illex illecebrosus[a]	Shortfin squid	0.190	0.015	. . .	48.19	108.73	255.66	Ganley *et al.*, 2023
I. illecebrosus[a]	Shortfin squid	. . .	0.5	. . .	90	. . .	. . .	Foyle and O'Dor, 1987
Doryteuthis pealeii[a]	Longfin squid	0.160	0.011	. . .	36.12	82.36	269.23	Ganley *et al.*, 2023
Sepia bandensis[a]	Dwarf cuttlefish	0.095	0.0012	0.00013	54.8	160.2	485.0	Jastrebsky *et al.*, 2016
S. bandensis[a]	Dwarf cuttlefish	0.142	0.0128	0.00036	45.85	110.34	910.5	This study
Sepia officinalis[a]	Common cuttlefish	. . .	. . .	. . .	~115	. . .	. . .	Messenger, 1968
Nanomia bijuga[a]	Siphonophore	0.150	. . .	0.05	104	215	363	Sutherland *et al.*, 2019
Aurelia aurita[a]	Moon jelly	. . .	. . .	. . .	. . .	~400	. . .	Dabiri *et al.*, 2020
Thunnus albacares	Albacore tuna	0.47	. . .	0.20	. . .	. . .	. . .	Blake *et al.*, 1995
Ostracion meleagris	Spotted boxfish	. . .	. . .	0.0005	. . .	. . .	218.4	Walker, 2000
Triakis semifasciata	Leopard shark	. . .	0.006	. . .	. . .	~300.2	. . .	Porter *et al.*, 2011
Chrysemys picta	Painted turtle	. . .	. . .	0.0018	. . .	. . .	291.6	Rivera *et al.*, 2006
Zalophus californianus	California sea lion	. . .	0.11	0.09	. . .	599	690	Fish *et al.*, 2003
Tursiops truncatus	Common bottlenose dolphin	0.21	. . .	0.08	561	. . .	1372	Maresh *et al.*, 2004
Dineutes horni	Whirligig beetle	0.86	. . .	0.24	1690.2	. . .	4428	Fish and Nicastro, 2003

$(R/L)_{mean}$, mean length-specific turning radius of a turn; $(R/L)_{min}$, minimum length-specific turning radius of a turn; Ω_{ave}, average angular velocity; Ω_{max}, maximum angular velocity. Values proceeded by an approximately sign (~) indicate where variables were approximated from data presented in the associated paper.

[a] Jet-propelled animals.

navigation in challenging environments, tracking prey, and communicating with conspecifics (Hanlon and Messenger, 1996; Hanlon *et al.*, 2018; Bartol *et al.*, 2022, 2023; Ganley *et al.*, 2023). Hydrodynamic parameters also varied greatly across individual *S. bandensis*, with each cuttlefish producing a large range of L_ω/D_ω and $\mathbf{A_{yaw}}$. Most cuttlefish produced jets with relatively low U_{jave} and U_{jmax}, including one cuttlefish (ID 1) that had the lowest average minimum turning radius ($(R/L)_{min} = 0.0013$) and some of the slowest angular and jet velocities ($\Omega_{ave} = 35.15°\ s^{-1}$; $U_{jave} = 2.74\ cm\ s^{-1}$). However, one cuttlefish had high jet velocities and still managed to turn relatively tightly. This cuttlefish (ID 3) had $U_{jave} > 30\ cm\ s^{-1}$ and $U_{jmax} \sim 45\ cm\ s^{-1}$ (Fig. 8). The high jet velocities translated to moderately high angular velocities ($\Omega_{ave} \sim 50$) and a fairly tight turning radius ($(R/L)_{mean} \sim 0.07$), suggesting that short, high-velocity, vectored jets can be effective for controlled, high-spin-rate turns.

Higher angular velocities for sequences without captured flow fields relative to those with flow fields was unexpected. These differences cannot be easily explained by laser-induced behavioral differences, as laser pulsing was present throughout all data collection periods. However, it is conceivable that the bias toward lower angular velocities (for sequences with captured flow fields) is a product of limitations in detecting higher-velocity jets that are presumably necessary for fast turns. Difficulties in detecting these jets could derive from an insufficiently short Δt or limitations in the 3D particle-tracking algorithms. However, missing vectors in the regions of jets were rare, and higher jet velocities have been detected using similar equipment and similar Δt (Bartol *et al.*, 2023); thus, it is unlikely that our approach failed to capture a significant number of high-velocity jets. It also may be that sampling volume size (14 cm × 14 cm × 10 cm) excludes some longer jet wakes used for high-angular-velocity turns, as only vortex flows that were fully visible and away from sampling volume boundaries were considered. Irrespective of the underlying cause, the observed difference in angular velocity between the datasets suggests that there may be some bias in kinematic

data when flow quantification data are collected simultaneously. Indeed, kinematic differences in datasets collected with and without flow field measurements have been reported in prior squid studies as well (*e.g.*, see Bartol *et al.*, 2023; Ganley *et al.*, 2023).

Comparison to other nekton

To better understand the abilities of turning cuttlefish, comparisons to taxa beyond cephalopods is necessary. *Sepia bandensis* in the present study turned more tightly (lower R/L) than most noncephalopod swimmers but turned slower (intermediate Ω) than some taxa (Table 3). The jet-propelled moon jelly, *Aurelia aurita*, is able to complete turns of relatively high angular velocities (peak $\Omega_{max} \sim 400° \ s^{-1}$), using asymmetric bell contraction to produce propulsive jets (Gemmell *et al.*, 2015; Dabiri *et al.*, 2020; Costello *et al.*, 2021). Another jet-propelled swimmer, the common siphonophore *Nanomia bijuga*, produces turns with $(R/L)_{mean} = 0.15$ and reaches average $\Omega_{max} = 215° \ s^{-1}$ (Sutherland *et al.*, 2019). While the average $(R/L)_{mean}$ of *N. bijuga* is similar to that of *S. bandensis* ($(R/L)_{mean} = 0.142$), *S. bandensis* achieves tighter turns at its performance extremes (*N. bijuga*: minimum $(R/L)_{min} = 0.05$; *S. bandensis*: minimum $(R/L)_{min} = 0.00036$; Table 2). Animals that do not use jet propulsion are also capable of tight turns, including the leopard shark, *Triakis semifasciata*, with average $(R/L)_{min} = 0.006$ (Porter *et al.*, 2011), which is lower than that reported in this study for *S. bandensis* (average $(R/L)_{min} = 0.0128$). The spotted boxfish, *Ostracion meleagris*, has been observed turning with $(R/L)_{min} = 0.0005$, which is the tightest length-specific turning radii reported for non–jet propulsors but is slightly wider than the tightest turns completed by *S. bandensis* and *L. brevis* (Walker, 2000; Jastrebsky *et al.*, 2016). Similarly, the painted turtle, *Chrysemys picta*, has $(R/L)_{min} = 0.0018$ at its performance extreme (Rivera *et al.*, 2006), which is significantly larger than the minimum $(R/L)_{min}$ reported in this study for *S. bandensis*. While *S. bandensis* turns tightly, it does so generally at low angular velocity. With an average Ω_{max} of $110° \ s^{-1}$, *S. bandensis* turns slower than the jet-propelled siphonophore *N. bijuga* ($215° \ s^{-1}$), Atlantic brief squid *L. brevis* ($268° \ s^{-1}$), leopard shark *T. semifasciata* ($\sim 300° \ s^{-1}$), and moon jelly *A. aurita* ($\sim 400° \ s^{-1}$) (Dabiri *et al.*, 2020; Jastrebsky *et al.*, 2016; Porter *et al.*, 2011; Sutherland *et al.*, 2019). Interestingly, *S. bandensis* in this study reached higher extreme Ω_{max} than all the previously mentioned taxa, indicating that *S. bandensis* is capable of high-speed turns but does not employ them often. This may be due to their use of crypsis as a first line of defense, which is often successful, eliminating the need for quick escape turns (Hanlon and Messenger, 1996; Bedore *et al.*, 2015). However, both bottlenose dolphins *Tursiops truncatus* ($1372° \ s^{-1}$) and whirligig beetles *Dineutes horni* ($4428° \ s^{-1}$) reach much higher Ω_{max} at their extremes than *S. bandensis*, but these fast-turning species have higher length-specific turning radii (*T. truncatus*: $(R/L)_{mean} = 0.21$; *D. horni*: $(R/L)_{mean} = 0.86$) (Fish and Nicastro, 2003; Maresh *et al.*, 2004) than *S. bandensis*.

Conclusions

Little is known about the kinematics and hydrodynamics of turning cuttlefish. The integrated approach (body tracking and 3D flow quantification) used in this study demonstrated that adult *S. bandensis* turn tightly but relatively slowly using short jet pulses, with orientation (arms-first *vs.* tail-first) not having a significant effect on performance or jet properties. Wake patterns were similar to those seen in other jet-propelled animals, but *S. bandensis* relied more heavily on jet mode I (>80% of turns), where jet flows rolled up into isolated vortex rings, and produced fewer complex jet signatures than squids. By using short ($L_\omega/D_\omega < 3$) vortex ring-based jets (jet mode I) in succession, *S. bandensis* achieved turns with R/L as low as 0.00036, which is among the lowest $(R/L)_{min}$ measured to date. These tight turns come with a trade-off, as *S. bandensis* generally completed these turns at low to moderate Ω. For broader turns, *S. bandensis* exhibited higher angular velocity, with $\Omega_{max} > 900° \ s^{-1}$.

Acknowledgments

We thank Amanda Tumminelli for her assistance in data collection. We also appreciate editorial suggestions from Dan Barshis, John Whiteman, Kent Carpenter, and Mike Vecchione. In addition, we thank the Marine Biological Laboratory, in Woods Hole, Massachusetts, for assistance in acquiring and guidance in caring for cuttlefish. This work was supported by the National Science Foundation (IOS 1557669 and 1557698 to IKB and PSK) as well as by the Graduate School Research Fellowship at Old Dominion University to AMG. We declare no competing interests. Author contributions are as follows: conceptualization: AMG, IKB, PSK; methodology: IKB, PSK; software: PSK; validation: AMG, IKB, PSK; formal analysis: AMG; investigation: AMG, IKB, PSK; resources: IKB, PSK; data curation: AMG; writing, original draft preparation: AMG; writing, review, and editing: AMG, IKB, PSK; visualization: AMG; supervision: IKB, PSK; project administration: IKB; funding acquisition: IKB, PSK, AMG.

Ethical Care Approval

This animal study was approved by Institutional Animal Care and Use Committee protocol 21-002 to IKB at Old Dominion University.

Literature Cited

Bartol, I. K., M. R. Patterson, and R. Mann.
2001. Swimming mechanics and behavior of the shallow-water brief squid *Lolliguncula brevis*. *J. Exp. Biol.* **204:** 3655–3682.

Bartol, I. K., P. S. Krueger, J. T. Thompson, and W. J. Stewart. 2008. Swimming dynamics and propulsive efficiency of squids throughout ontogeny. *Integr. Comp. Biol.* **48:** 720–733.

Bartol, I. K., P. S. Krueger, W. J. Stewart, and J. T. Thompson. 2009a. Hydrodynamics of pulsed jetting in juvenile and adult brief squid *Lolliguncula brevis*: evidence of multiple jet "modes" and their implications for propulsive efficiency. *J. Exp. Biol.* **212:** 1889–1903.

Bartol, I. K., P. S. Krueger, W. J. Stewart, and J. T. Thompson. 2009b. Pulsed jet dynamics of squid hatchlings at intermediate Reynolds numbers. *J. Exp. Biol.* **212:** 1506–1518.

Bartol, I. K., P. S. Krueger, R. A. Jastrebsky, S. Williams, and J. T. Thompson. 2016. Volumetric flow imaging reveals the importance of vortex ring formation in squid swimming tail-first and arms-first. *J. Exp. Biol.* **219:** 392–403.

Bartol, I. K., P. S. Krueger, C. A. York, and J. T. Thompson. 2018. New approaches for assessing squid fin motions: coupling proper orthogonal decomposition with volumetric particle tracking velocimetry. *J. Exp. Biol.* **222:** jeb176750.

Bartol, I. K., A. M. Ganley, A. N. Tumminelli, P. S. Krueger, and J. T. Thompson. 2022. Vectored jets power arms-first and tail-first turns differently in brief squid with assistance from fins and keeled arms. *J. Exp. Biol.* **225:** jeb244151.

Bartol, I. K., A. M. Ganley, A. N. Tumminelli, S. M. Bartol, J. T. Thompson, and P. S. Krueger. 2023. Turning performance and wake dynamics of neritic squids. *Mar. Biol.* **170:** 73.

Bedore, C. N., S. M. Kajiura, and S. Johnsen. 2015. Freezing behaviour facilitates bioelectric crypsis in cuttlefish faced with predation risk. *Proc. R. Soc. B* **282:** 20151886.

Blake, R. W., L. M. Chatters, and P. Domenici. 1995. Turning radius of yellowfin tuna (*Thunnus albacares*) in unsteady swimming manoeuvres. *J. Fish Biol.* **46:** 536–538.

Budick, S. A., and D. M. O'Malley. 2000. Locomotor repertoire of the larval zebrafish: swimming, turning and prey capture. *J. Exp. Biol.* **203:** 2565–2579.

Catano, L. B., B. K. Gunn, M. C. Kelley, and D. E. Burkepile. 2015. Predation risk, resource quality, and reef structural complexity shape territoriality in a coral reef herbivore. *PLoS One* **10:** e0118764.

Catano, L. B., M. C. Rojas, R. J. Malossi, J. R. Peters, M. R. Heithaus, J. W. Fourqurean, and D. E. Burkepile. 2016. Reefscapes of fear: predation risk and reef hetero-geneity interact to shape herbivore foraging behaviour. *J. Anim. Ecol.* **85:** 146–156.

Colin, S. P., J. H. Costello, K. Katija, J. Seymour, and K. Kiefer. 2013. Propulsion in Cubomedusae: mechanisms and utility. *PLoS One* **8:** e56393.

Costello, J. H., S. P. Colin, B. J. Gemmell, J. O. Dabiri, and K. R. Sutherland. 2015. Multi-jet propulsion organized by clonal development in a colonial siphonophore. *Nat. Commun.* **6:** 8158.

Costello, J. H., S. P. Colin, J. O. Dabiri, B. J. Gemmell, K. N. Lucas, and K. R. Sutherland. 2021. The hydrodynamics of jellyfish swimming. *Annu. Rev. Mar. Sci.* **13:** 375–396.

Couch, L. D., and P. S. Krueger. 2011. Experimental investigation of vortex rings impinging on inclined surfaces. *Exp. Fluids* **51:** 1123–1138.

Coughlin, D. J. 2000. Power production during steady swimming in largemouth bass and rainbow trout. *J. Exp. Biol.* **203:** 617–629.

Coughlin, D. J., and L. C. Rome. 1996. The roles of pink and red muscle in powering steady swimming in scup, *Stenotomus chrysops*. *Am. Zool.* **36:** 666–677.

Dabiri, J. O. 2009. Optimal vortex formation as a unifying principle in biological propulsion. *Annu. Rev. Fluid Mech.* **41:** 17–33.

Dabiri, J. O., S. P. Colin, J. H. Costello, and M. Gharib. 2005. Flow patterns generated by oblate medusan jellyfish: field measurements and laboratory analyses. *J. Exp. Biol.* **208:** 1257–1265.

Dabiri, J. O., S. P. Colin, B. J. Gemmell, K. N. Lucas, M. C. Leftwich, and J. H. Costello. 2020. Jellyfish and fish solve the challenges of turning dynamics similarly to achieve high maneuverability. *Fluids* **5:** 106.

Danos, N., and G. V. Lauder. 2007. The ontogeny of fin function during routine turns in zebrafish *Danio rerio*. *J. Exp. Biol.* **210:** 3374–3386.

Denton, E. J., and J. B. Gilpin-Brown. 1961. The buoyancy of the cuttlefish. *J. Mar. Biol. Assoc.* **41:** 319–342.

Dickel, L., A. S. Darmaillacq, R. Poirier, V. Agin, C. Bellanger, and R. Chichery. 2006. Behavioural and neural maturation in the cuttlefish *Sepia officinalis*. *Vie Milieu* **56:** 89–95.

Drucker, E. G., and G. V. Lauder. 2001. Wake dynamics and fluid forces of turning maneuvers in sunfish. *J. Exp. Biol.* **204:** 431–442.

Ellerby, D. J., I. L. Y. Spierts, and J. D. Altringham. 2022. Slow muscle power output of yellow- and silver-phase European eels (*Anguilla anguilla* L.): changes in muscle performance prior to migration. *J. Exp. Biol.* **204:** 1369–1379.

Epps, B. P., and A. H. Techet. 2007. Impulse generated during unsteady maneuvering of swimming fish. *Exp. Fluids* **43:** 691–700.

Finke, E., H. O. Pörtner, P. G. Lee, and D. M. Webber. 1996. Squid (*Lolliguncula brevis*) life in shallow waters: oxygen limitation of metabolism and swimming performance. *J. Exp. Biol.* **199:** 911–921.

Fish, F. E. 1999. Performance constraints on the maneuverability of flexible and rigid biological systems. Pp. 394–406 in *Proceedings of the Eleventh International Symposium on Unmanned Untethered Submersible Technology*, Durham, NC.

Fish, F. E. 2002. Balancing requirements for stability and maneuverability in cetaceans. *Integr. Comp. Biol.* **42:** 85–93.

Fish, F. E., and R. Holzman. 2019. Swimming turned on its head: stability and maneuverability of the shrimpfish (*Aeoliscus punctulatus*). *Integr. Org. Biol.* **1:** obz025.

Fish, F. E., and A. J. Nicastro. 2003. Aquatic turning performance by the whirligig beetle: constraints on maneuverability by a rigid biological system. *J. Exp. Biol.* **206:** 1649–1656.

Fish, F. E., J. Hurley, and D. P. Costa. 2003. Maneuverability by the sea lion *Zalophus californianus*: turning performance of an unstable body design. *J. Exp. Biol.* **206:** 667–674.

Fish, F. E., A. Kolpas, A. Crossett, M. A. Dudas, K. W. Moored, and H. Bart-Smith. 2018. Kinematics of swimming of the manta ray: three-dimensional analysis of open-water maneuverability. *J. Exp. Biol.* **221:** jeb166041.

Foyle, T. P., and R. K. O'dor. 1987. Predatory strategies of squid (*Illex illecebrosus*) attacking small and large fish. *Mar. Behav. Physiol.* **13:** 155–168.

Fuiman, L. A., and P. W. Webb. 1988. Ontogeny of routine swimming activity and performance in zebra danios (Teleostei: Cyprinidae). *Anim. Behav.* **36:** 250–261.

Ganley, A. M., P. S. Krueger, and I. K. Bartol. 2023. Faster is not always better: turning performance trade-offs in the inshore squids *Doryteuthis pealeii* and *Illex illecebrosus*. *J. Exp. Mar. Biol. Ecol.* **565:** 151913.

Ganley, A. M., P. S. Krueger, and I. K. Bartol. 2024. Baby's first jets: a kinematic and hydrodynamic analysis of turning in cuttlefish hatchlings. *Mar. Biol.* **171:** 221.

Gemmell, B. J., D. R. Troolin, J. H. Costello, S. P. Colin, and R. A. Satterlie. 2015. Control of vortex rings for manoeuvrability. *J. R. Soc. Interface* **12:** 20150389.

Gharib, M., E. Rambod, and K. Shariff. 1998. A universal time scale for vortex ring formation. *J. Fluid Mech.* **360:** 121–140.

Gladman, N. W., and G. N. Askew. 2023. The hydrodynamics of jet propulsion swimming in hatchling and juvenile European common cuttlefish *Sepia officinalis*, Linnaeus (1758). *J. Exp. Biol.* **226:** jeb.246225.

Good, J. T., M. R. Kendrick, R. D. Podolsky, J. D. Whitaker, and P. R. Kingsley-Smith. 2023. Life history patterns of the Atlantic brief squid, *Lolliguncula brevis* (Blainville, 1823), in the Charleston Harbor estuary, South Carolina, USA. *J. Shellfish Res.* **42:** 113–123.

Guerra, A. 2006. Ecology of *Sepia officinalis*. *Vie Milieu* **56:** 97–107.

Hanlon, R. T., and J. B. Messenger. 1996. *Cephalopod Behaviour*. Cambridge University Press, New York.

Hanlon, R. T., R. F. Hixon, and W. H. Hulet. 1983. Survival, growth, and behavior of the loliginid squids *Loligo plei*, *Loligo pealei*, and *Lolliguncula brevis* (Mollusca: Cephalopoda) in closed sea water systems. *Biol. Bull.* **165:** 637–685.

Hanlon, R. T., M. Vecchione, and L. Allcock. 2018. *Octopus, Squid, and Cuttlefish*. Quarto, Chicago.

Hedrick, T. L. 2008. Software techniques for two- and three-dimensional kinematic measurements of biological and biomimetic systems. *Bioinspir. Biomim.* **3:** 034001.

Hoar, J. A. 1995. The changing role of fins in growing loliginid squid (Mollusca; Cephalopoda). PhD dissertation, Dalhousie University, Halifax, Nova Scotia.

Jastrebsky, R. A., I. K. Bartol, and P. S. Krueger. 2016. Turning performance in squid and cuttlefish: unique dual-mode, muscular hydrostatic systems. *J. Exp. Biol.* **219:** 1317–1326.

Jastrebsky, R. A., I. K. Bartol, and P. S. Krueger. 2017. Turning performance of brief squid *Lolliguncula brevis* during attacks on shrimp and fish. *J. Exp. Biol.* **220:** jeb.144261.

Jayne, B. C., and G. V. Lauder. 1995. Are muscle fibers within fish myotomes activated synchronously? Patterns of recruitment within deep myomeric musculature during swimming in largemouth bass. *J. Exp. Biol.* **198:** 805–815.

Jereb, P., and C. F. E. Roper. 2005. *An Annotated and Illustrated Catalogue of Species Known to Date.* Food and Agriculture Organization of the United Nations, Rome.

Johnson, T. P., D. A. Syme, B. C. Jayne, G. V. Lauder, and A. F. Bennett. 1994. Modeling red muscle power output during steady and unsteady swimming in largemouth bass. *Am. J. Physiol. Integr. Comp. Physiol.* **267:** R481–R488.

Kier, W. M. 1989. The fin musculature of cuttlefish and squid (Mollusca, Cephalopoda): morphology and mechanics. *Zool. Soc. Lond.* **217:** 23–38.

Kier, W. M., and J. T. Thompson. 2003. Muscle arrangement, function and specialization in recent coleoids. *Berl. Palaeobiol. Abh.* **3:** 141–162.

Kobayashi, S., C. Takayama, and Y. Ikeda. 2013. Ontogeny of the brain in oval squid *Sepioteuthis lessoniana* (Cephalopoda: Loliginidae) during the

post-hatching phase. *J. Mar. Biol. Assoc. UK* **93:** 1663–1671.

Krueger, P. S., and M. Gharib. 2003. The significance of vortex ring formation to the impulse and thrust of a starting jet. *Phys. Fluids* **15:** 1271–1281.

Lauder, G. V., and E. G. Drucker. 2002. Forces, fishes, and fluids: hydrodynamic mechanisms of aquatic locomotion. *News Physiol. Sci.* **17:** 235–240.

Linden, P. F., and J. S. Turner. 2004. "Optimal" vortex rings and aquatic propulsion mechanisms. *Proc. R. Soc. B* **271:** 647–653.

Liu, Y. C., T. H. Liu, C. H. Su, and C. C. Chiao. 2017. Neural organization of the optic lobe changes steadily from late embryonic stage to adulthood in cuttlefish *Sepia pharaonis*. *Front. Physiol.* **8:** 538.

Maresh, J. L., F. E. Fish, D. P. Nowacek, S. M. Nowacek, and R. S. Wells. 2004. High performance turning capabilities during foraging by bottlenose dolphins (*Tursiops truncatus*). *Mar. Mamm. Sci.* **20:** 498–509.

Messenger, J. B. 1968. The visual attack of the cuttlefish, *Sepia officinalis*. *Anim. Behav.* **16:** 342–357.

Müller, U. K., and D. Lentink. 2004. Turning on a dime. *Science* **306:** 1899–1900.

Müller, U. K., J. G. M. Van Den Boogaart, and J. L. Van Leeuwen. 2008. Flow patterns of larval fish: undulatory swimming in the intermediate flow regime. *J. Exp. Biol.* **211:** 196–205.

Parson, J. M., F. E. Fish, and A. J. Nicastro. 2011. Turning performance of batoids: limitations of a rigid body. *J. Exp. Mar. Biol. Ecol.* **402:** 12–18.

Pereira, F., M. Gharib, D. Dabiri, and D. Modarress. 2000. Defocusing digital particle image velocimetry: a 3-component 3-dimensional DPIV measurement technique: application to bubbly flows. *Exp. Fluids* **29:** S078–S084.

Pereira, F., H. Stüer, E. C. Graff, and M. Gharib. 2006. Two-frame 3D particle tracking. *Meas. Sci. Technol.* **17:** 1680–1692.

Porter, M. E., C. M. Roque, and J. H. Long. 2011. Swimming fundamentals: Turning performance of leopard sharks (*Triakis semifasciata*) is predicted by body shape and postural reconfiguration. *Zoology* **114:** 348–359.

Rivera, G., A. R. V. Rivera, E. E. Dougherty, and R. W. Blob. 2006. Aquatic turning performance of painted turtles (*Chrysemys picta*) and functional consequences of a rigid body design. *J. Exp. Biol.* **209:** 4203–4213.

Rizzari, J. R., A. J. Frisch, A. S. Hoey, and M. I. McCormick. 2014. Not worth the risk: Apex predators suppress herbivory on coral reefs. *Oikos* **123:** 829–836.

Rome, L. C., D. Swank, and D. Corda. 1993. How fish power swimming. *Science* **261:** 340–343.

Saffman, P. G. 1995. *Vortex Dynamics*. Cambridge University Press, Cambridge.

Stewart, W. J., I. K. Bartol, and P. S. Krueger. 2010. Hydrodynamic fin function of brief squid, *Lolliguncula brevis*. *J. Exp. Biol.* **213:** 2009–2024.

Sutherland, K. R., B. J. Gemmell, S. P. Colin, and J. H. Costello. 2019. Maneuvering performance in the colonial siphonophore, *Nanomia bijuga*. *Biominetics* **4:** 62.

Thandiackal, R., and G. V. Lauder. 2020. How zebrafish turn: analysis of pressure force dynamics and mechanical work. *J. Exp. Biol.* **223:** jeb223230.

Thompson, J. T., and W. M. Kier. 2001. Ontogeny of squid mantle function: changes in the mechanics of escape-jet locomotion in the oval squid, *Sepioteuthis lessoniana* Lesson, 1830. *Biol. Bull.* **203:** 14–26.

Thompson, J. T., and W. M. Kier. 2006. Ontogeny of mantle musculature and implications for jet locomotion in oval squid *Sepioteuthis lessoniana*. *J. Exp. Biol.* **209:** 433–443.

Troolin, D. R., and E. K. Longmire. 2009. Volumetric velocity measurements of vortex rings from inclined exits. *Exp. Fluids* **48:** 409–420.

Walker, J. A. 1998. Estimating velocities and accelerations of animal locomotion: a simulation experiment comparing numerical differentiation algorithms. *J. Exp. Biol.* **201:** 981–995.

Walker, J. A. 2000. Does a rigid body limit maneuverability? *J. Exp. Biol.* **203:** 3391–3396.

Webb, P. W., and P. T. Kostecki. 1984. The effect of size and swimming speed on locomotor kinematics of rainbow trout. *J. Exp. Biol.* **109:** 77–95.

Weihs, D. 1972. A hydrodynamical analysis of fish turning manoeuvres. *Proc. R. Soc. B* **182:** 59–72.

Wu, J.-Z., H.-Y. Ma, and M.-D. Zhou. 2007. *Vorticity and Vortex Dynamics*. Springer Science and Business, Berlin.